Innovative operational strategies in photosynthetic biogas upgrading in an outdoors pilot scale algal-bacterial photobioreactor

David Marín[1, 2, 3], Alessandro A. Carmona-Martínez[1, 2], Saúl Blanco[4], Raquel Lebrero[1, 2], Raúl Muñoz*[1, 2]

[1] Department of Chemical Engineering and Environmental Technology, School of Industrial Engineering, Valladolid University, Dr. Mergelina, s/n, 47011, Valladolid, Spain.

[2] Institute of Sustainable Processes, Dr. Mergelina, s/n, 47011, Valladolid, Spain.

[3] Universidad Pedagógica Nacional Francisco Morazán, Boulevard Centroamérica, Tegucigalpa, Honduras.

[4] Department of Biodiversity and Environmental Management, University of León, 24071 León, Spain.

* Corresponding author: mutora@iq.uva.es

ABSTRACT

Three innovative operational strategies were successfully evaluated to improve the quality of biomethane in an outdoors pilot scale photobioreactor interconnected to an external absorption unit: i) the use of a greenhouse during winter conditions, ii) a direct CO_2 stripping in the photobioreactor via air stripping during winter conditions and iii) the use of digestate as make-up water during summer conditions. CO_2 concentrations in the biomethane ranged from 0.4% to 6.1% using the greenhouse, from 0.3% to 2.6% when air was injected in the photobioreactor and from 0.4% to 0.9% using digestate as make up water. H_2S was completely removed under all strategies tested. On the other hand, CH_4 concentrations in biomethane ranged from 89.5% to 98.2%, from 93.0% to 98.2% and from 96.3% to 97.9%, when implementing strategies i), ii) and iii), respectively. The greenhouse was capable of maintaining microalgae productivities of 7.5 g m^{-2} d^{-1} during continental weather conditions, while mechanical CO_2 stripping increased the pH in order to support an effective CO_2 and H_2S removal. Finally, the high evaporation rates during

summer conditions allowed maintaining high inorganic carbon concentrations in the cultivation broth using centrate, which provided a cost-effective biogas upgrading.

Keywords:

Algal bacterial photobioreactor; Biogas upgrading; Greenhouse; Innovative operational strategies; Outdoors conditions

1. Introduction

Biogas originating at the anaerobic treatment of wastewater and organic waste represents a renewable energy vector capable of reducing the use of fossil fuels to satisfy the demand of electricity and heat for domestic and industrial applications (Muñoz et al., 2015). Biogas upgrading is required prior use as vehicle fuel or it is injection into gas network due to the high concentration of impurities present in raw biogas such as CO_2 (15-60%), CO (<0.6%), O_2 (0-1%), N_2 (0-2%), H_2S (0.005-2%), siloxanes (0-0.2%), NH_3 (<1%) and volatile organic compounds (<0.6%) (Ryckebosch et al., 2011). Typical compositions in biomethane varies depending on the national regulations or regional standards: $CH_4 \geq$ 90-95%, $CO_2 \leq$ 2-4%, $O_2 \leq$ 1% and insignificant amounts of H_2S (Muñoz et al., 2015). In this context, the relevance of biogas and biomethane in the EU energy sector has increased within the past years as result of the active policies for decarbonization of European economy. Indeed, the number of biogas plants has escalated from 6227 in 2009 to 17783 by the end of 2017, while biomethane production capacity has escalated from 752 GWh by 2011 to 19352 GWh by the end of 2017 (European Biogas Association, 2018).

Multiple physicochemical technologies existing at present are commercially available to remove CO_2 and H_2S from biogas in order to comply with biomethane standards. Pressure swing adsorption, water/chemical/organic scrubbing, membrane separation, or cryogenic separation provide the required levels of CO_2 removal at energy demands ranging from 0.3-0.8 kWh Nm^{-3}. *In-situ* chemical precipitation or adsorption onto activated carbon or metal ions provide the required levels of H_2S removal at operating costs in the range of 2-3 € cent Nm^{-3} (Angelidaki et al., 2018; Marín et al., 2019; Muñoz et al., 2015; Rodero et al., 2018). An integral upgrading of biogas to comply with biomethane standards requires the sequential combination of these H_2S and CO_2 removal technologies, which significantly increases the initial investment and operational fees of the process (nowadays accounting for ~30 % of the biomethane price (Stürmer et al., 2016)). The urgent need to decrease the cost and energy demand of conventional biogas upgrading has triggered research on biological methods for CO_2 and H_2S removal. Chemoautotrophic biogas upgrading can support the required levels of CO_2 bioconversion to CH_4 with renewable H_2, while *in-situ* micro-aerobic anaerobic digestion or biofiltration can provide a cost-effective H_2S removal (Farooq et al., 2018; Marín et al., 2018a; Muñoz et al., 2015; Rodero et al., 2018). However, algal-bacterial photobioreactors constitute the only biological alternative to conventional physical-chemical processes capable of simultaneously removing CO_2 and H_2S in a single step process at low operating costs (Bahr et al., 2014; Bose et al., 2019; Muñoz et al., 2015; Nagarajan et al., 2019).

Photosynthetic biogas upgrading processes using algal-bacterial photobioreactors are based on the fixation of CO_2 by microalgae using solar energy and the aerobic oxidation of H_2S to SO_4^{2-} by sulfur oxidizing bacteria mediated by the elevated dissolved oxygen

(DO) concentrations in the photobioreactor as a result of photosynthetic activity (Posadas et al., 2015; Toledo-Cervantes et al., 2016). Photosynthetic biogas upgrading processes have been previously optimized in commercially interconnected to external biogas absorption columns under indoors conditions and with artificial illumination (Bahr et al., 2014; Franco-Morgado et al., 2017; Posadas et al., 2016; Rodero et al., 2018; Serejo et al., 2015). In addition, these processes have been validated under outdoors conditions in multiple photobioreactor configurations. For instance, Posadas et al., (2017) evaluated for the first time the upgrading of biogas and centrate treatment in a 180 L commercially during summer time. Marín et al., (2018b, 2018a) assessed the impact of seasonal variations of environmental conditions on biogas upgrading performance in a 180 L commercially fed with HCO_3^-/CO_3^{2-} supplemented digestate. Similarly, Marín et al., (2019) investigated the impact of the liquid to biogas flowrate (L/G) ratio and alkalinity in the cultivation broth on the quality of biomethane in a 11.7 m^3 horizontal hybrid tubular photobioreactor. Despite the satisfactory results obtained to date, the photosynthetic biogas upgrading processes under outdoor conditions is limited by the low temperatures during winter conditions under continental climate and the need for external alkalinity sources. Therefore, innovative operating strategies are needed to provide a cost-effective photosynthetic biogas upgrading during unfavorable environmental conditions and without external alkalinity supplementation (Toledo-cervantes et al., 2017).

This study investigated, for the first time, the performance of three innovative operational strategies in order to improve the quality of biomethane and process sustainability in an outdoors pilot scale photobioreactor interconnected to an external absorption unit. These strategies aimed at overcoming previous limitations encountered during process validation under outdoors conditions (Marin et al. 2018). For this purpose, the outdoors

pilot photobioreactor interconnected to an external biogas scrubbing unit was located inside of a greenhouse during winter conditions. The potential of direct CO_2 stripping in the photobioreactor via air stripping during winter conditions and of the use of digestate as make-up water (to compensate water losses by evaporation) during summer conditions to improve the quality of biomethane were evaluated.

2. Materials and methods

2.1 Biogas and synthetic digestate

A synthetic gas mixture composed of CH_4 (70%), CO_2 (29.5%) and H_2S (0.5%) was used as a raw biogas in the present study (Abello Linde; Spain). The synthetic digestate (SWW) used during the first 225 days of experiment consisted of (per liter of distilled water): 7.40 g $NaHCO_3$, 3.70 g Na_2CO_3, 0.94 g K_2HPO_4, 1.91 g NH_4Cl, 0.02 g $CaCl_2 \cdot 2H_2O$, 0.005 g $FeSO_2 \cdot 7H_2O$, 0.10 g $MgSO_4 \cdot 7H_2O$ and 5 ml of a micronutrient solution (composed of 0.10 g $ZnSO_4 \cdot 7H_2O$, 0.10 g $MnCl_2 \cdot 4H_2O$, 0.20 g H_3BO_3, 0.02 g $Co(NO_3)_2 \cdot 6H_2O$, 0.02 g $Na_2MoO_4 \cdot 2H_2O$, 0.0005 g $CuSO_4 \cdot 5H_2O$, 0.70 g $FeSO_4 \cdot 7H_2O$ and 1.02 g $EDTA \cdot 2Na \cdot 2H_2O$ per liter of distilled water). This resulted in an inorganic carbon (IC) concentration of 1500 ± 43 mg L^{-1}, total organic carbon (TOC) concentration of 54 ± 4 mg L^{-1}, total nitrogen (TN) concentration of 530 ± 19 mg L^{-1}, $P\text{-}PO_4^{3-}$ concentration of 94 ± 8 mg L^{-1} and $S\text{-}SO_4^{2-}$ concentration of 112 ± 7 mg L^{-1}. During the last 25 days of experiment, the IC concentration of the SWW was decreased to 532 ± 24 mg L^{-1} in order to mimic the typical composition of centrate from Valladolid wastewater treatment plant.

2.2 Experimental set-up

The photobioreactor set-up was located outdoors at the Institute of Sustainable Processes of Valladolid University. The experimental set-up was integrated by a 180 L

126 photobioreactor divided in two water channels and with one baffle at each site of the
127 photobioreactor. The photobioreactor has an illuminated surface of 1.20 m^2 (length = 170
128 cm; depth = 15 cm; width = 82 cm). The cultivation broth inside the photobioreactor was
129 recirculated with a velocity of 20 cm s^{-1} by a 6-blade paddlewheel. An absorption unit of
130 2.5 L was interconnected to the photobioreactor through a conical settler of 8 L. A
131 metallic diffuser of 2 µm pore size was installed at the bottom of the biogas scrubbing
132 column. The photobioreactor was installed inside of a greenhouse in order to enhance the
133 performance of the technology during winter conditions (Fig. 1). From day 99 until day
134 225 of experiment, air was injected directly into the photobioreactor via 3 porous stone
135 diffusers evenly distributed along the photobioreactor.

136 **<Figure 1>**

137

138 **2.3 Operational conditions and sampling procedures**

139 The photobioreactor was inoculated with a microalgal inoculum composed of
140 *Mychonastes homosphaera (82%), Pseudanabaena sp. (17%) and Scenedesmus sp. (1%)*
141 (percentages are expressed in number of cells) to a concentration of 450 mg total
142 suspended solids (TSS) L^{-1}. Five stages (namely A, B, C, D and E) were defined as a
143 function of the operational conditions (Table 1). The SWW used as a source of nutrients
144 was fed to the photobioreactor at a flow rate of 3.5 L d^{-1}. Meanwhile, biogas was injected
145 at the bottom of the absorption unit at a flow rate of 72 L d^{-1} under co-current flow
146 operation with a L/G ratio of 1.0 (Posadas et al., 2017). Tap water (days 99 – 198), highly
147 carbonated SWW (days 199 – 225) and SWW (days 226 – 250) were supplied in order to
148 compensate water evaporation losses but allowing process operation without effluent. Air
149 was injected in the photobioreactor at a flow rate of 8.0 L min^{-1} from days 99 to 225 in
150 order to evaluate the influence of mechanical CO_2 stripping in the photobioreactor on

biomethane quality. Biomass productivity was fixed according to the environmental conditions present at each operational stage in order to provide a constant growth of microalgae during stages A (0.0 g m^{-2} d^{-1}), B and C (7.5 g m^{-2} d^{-1}) and D and E (15.0 g m^{-2} d^{-1}) (Table 1). Harvesting of algae-bacteria from the settler was carried out to maintain this productivity. The remaining biomass at the bottom of the settler was recirculated to the photobioreactor at a flow rate of 3.6 or 7.2 L d^{-1}.

<Table 1>

The photosynthetic active radiation (PAR) outdoors and inside the greenhouse, the temperature outdoors, inside the greenhouse and in the photobioreactor and the DO concentration were daily monitored at 9:00 a.m and 4:00 p.m throughout the entire experimental period. The pH was daily measured only at 9:00 a.m since it remained constant throughout the daytime as a result of the high buffer capacity of the cultivation broth (Marín et al., 2018b). In order to measure IC, TOC, TN, $N\text{-}NO_3^-$, $N\text{-}NO_2^-$, $P\text{-}PO_4^{3-}$, $S\text{-}SO_4^{2-}$ and biomass concentrations, 100 mL of liquid samples from the photobioreactor and the SWW were drawn twice a week. In order to determine CH_4, CO_2, H_2S, N_2 and O_2 concentrations in raw biogas and biomethane, gas samples of 100 µL were taken in duplicate at 10:00 a.m twice a week. At each month, samples of the photobioreactor were taken in order to morphologically determine the structure of microalgae population.

2.4 Analytical procedures

PAR, pH, temperature and DO concentration were recorded according to Marín et al., (2018a). The concentrations of TOC, IC and TN were analyzed according to Posadas et al., (2017). $N\text{-}NO_3^-$, $N\text{-}NO_2^-$, $P\text{-}PO_4^{3-}$ and $S\text{-}SO_4^{2-}$ concentrations were quantified by HPLC-IC according to Posadas et al., (2013). The determination of TSS and VSS concentrations was carried out according to APHA (2005). Biogas and biomethane

composition were determined according to Marín et al., (2018a). The determination of the N and P content of the algal bacterial biomass was determined according to Posadas et al., (2017). Finally, the identification, quantification and biometry measurements of microalgae were conducted by microscopic examination (OLYMPUS IX70, USA) of the algal–bacterial cultivation broths (fixed with lugol acid at 5% and stored at 4ºC prior to analysis) according to Sournia (1978). The microalgae growing on each unit were identified and quantified according to the European standard CEN TC 230/WG2/TG3/N83, which is based on Utermöhl´s (1958) method.

3. Results and discussion

3.1 Environmental parameters

Considerable variations in the ambient, greenhouse and photobioreactor temperatures were recorded in the course of the experimental time due to the seasonal climate variation. The ambient temperature recorded in stages A, B, C, D and E ranged from 4.0 to 23.0, -3.0 to 17.0, -3.0 to 23.0, 7.0 to 27.0 and 7.0 to 30.0 ºC, respectively (Fig. 2a). This ambient temperature influenced directly the temperatures recorded inside the greenhouse, which ranged from 5.0 to 40.0, -4.0 to 26.0 and -2.0 to 43.0 ºC in stages A, B and C, respectively (Fig. 2b). The greenhouse was responsible of the difference of temperatures due to its inherent ability to retain solar radiation. This increase in the temperature of the greenhouse exerted an important effect in the temperature of the photobioreactor. Hence, the photobioreactor temperature recorded in stages A, B, C, D and E ranged from 4.2 to 24.1, -0.2 to 18.7, 0.5 to 31.7, 6.1 to 27.6 and 8.1 to 32.2 ºC, respectively (Fig. 2c). The temperature values here reported during winter time were significantly higher than those previously recorded by Marín et al., (2018a) in the same period (2.3 ± 3.1 ºC), and prevent the freezing of the photobioreactor.

<Figure 2>

The ambient PAR recorded in stages A, B, C, D and E ranged from 26 to 966, 24 to 790, 27 to 1738, 65 to 1684 and 76 to 1549 µmol m^{-2} s^{-1}, respectively (Fig. 2d). The plastic material of the greenhouse produced a significant decrease in the PAR recorded inside during stages A, B and C, which ranged from 17 to 807, 12 to 422 and 17 to 1024 µmol m^{-2} s^{-1}, respectively (Fig. 2e). Overall, the average decrease in PAR during the daytime was 36% along the three initial stages carried out inside the greenhouse. It is important to stress that these differences in PAR among the three initial stages were inherent to the seasonal variability of the environmental conditions throughout the experimental period. Environmental parameters such as temperature and PAR governed the biomass productivity set (and controlled via biomass wasting through the settler) at each stage, which was gradually increased from 0.0 to 15.0 g m^{-2} d^{-1} (Table 1), in accordance with Marín et al., (2018a) and Posadas et al., (2017) in a similar photobioreactor under outdoor conditions.

The gradual increases in ambient temperature and ambient PAR during the experimentation time were correlated with the evaporation rate from the cultivation broth of the photobioreactor. The average evaporation rates recorded in stages A, B, C, D and E were 1.7 ± 1.2, 1.1 ± 0.4, 2.4 ± 1.0, 5.2 ± 1.2 and 7.3 ± 1.1 L m^{-2} d^{-1}, respectively (Table 1; Fig. S1). The greenhouse prevented the external input of water from rain into the photobioreactor, which resulted in positive evaporation rates values throughout the entire experiment. In this context, Marín et al., (2018a) reported an evaporation rate value of -0.3 ± 1.8 L m^{-2} d^{-1} in a 180 L outdoors photobioreactor during winter time in Valladolid, while Rodero et al., (2019) reported rain inputs of 4.4 L m^{-2} d^{-1} in a 9.6 m^3 outdoors

225 photobioreactor in Chiclana de la Frontera (Spain), which resulted in evaporation rates
226 of -0.1 ± 0.6 L m^{-2} d^{-1}.
227
228 Finally, the mean DO concentrations recorded in stages A, B, C, D and E in the morning
229 accounted for 8.2 ± 2.2, 9.2 ± 1.7, 10.6 ± 0.8, 9.8 ± 0.7 and 7.7 ± 0.6 mg L^{-1}, respectively.
230 In the afternoon, the average values were 12.5 ± 5.5, 12.8 ± 1.4, 9.2 ± 1.1, 8.2 ± 0.2 and
231 7.3 ± 0.3 mg L^{-1}, respectively (Table 1; Fig. S2). The high DO values here reported as a
232 result of the low oxygen demand of the synthetic digestate used did not inhibit the
233 photosynthetic activity of microalgae. In this context, Molina et al., (2001) reported that
234 outdoors *Spirulina* productivities increased when the DO concentration decreased from
235 35 to 20 mg O_2 L^{-1}. The lower DO concentrations recorded under favorable
236 environmental conditions (stages D and E) were likely due to the higher endogenous
237 respiration, which supported an active oxygen demand to oxidize the intracellular
238 reserves of algae and bacteria for cell maintenance, mediated by the higher biomass
239 concentrations prevailing in the cultivation broth (approx. 3 times higher than in stages
240 A, B and C) and the higher ambient temperature that decreased DO in equilibrium with
241 air and accelerated biological reactions.
242
243 **3.2 Photobioreactor parameters**
244 The pH in the photobioreactor remained fairly constant throughout stage A and B, with
245 an average value of 9.1 ± 0.1, as consequence of the high buffer capacity of the cultivation
246 broth (Fig. 3a). In stage C and D, the injection of air directly into the photobioreactor
247 caused a gradual increase in the pH up to 9.9 as a result of a direct CO_2 stripping in the
248 microalgae medium of the photobioreactor (Fig 3a). Finally, the pH remained constant at
249 9.8 ± 0.1 in stage E. This high pH in the absence of air stripping was likely due to the

high photosynthetic activity of microalgae and the high IC concentration prevailing in the the photobioreactor mediated by the high evaporation rates.

<Figure 3>

The IC concentration in the photobioreactor fluctuated during stages A and B, with an average value of 1332 ± 87 mg L^{-1} (Fig. 3b). A gradual increase in the IC concentration up to 1639 mg L^{-1} was observed in stage C likely due to the increase in pH induced by the injection of air directly into the photobioreactor. A rapid increase in the IC concentration up to 1952 mg L^{-1} was recorded during stage D mediated by the increase in water evaporation losses caused by the higher temperatures and removal of the greenhouse (Fig. 3b; Table 1). Interestingly, the external supply of air in the photobioreactor directly impacted on the pH and IC concentration of the cultivation broth, but it did not increase the evaporation rate. The increase in the evaporation rate was correlated to the gradual increase in ambient temperature and PAR during the experimental period. Despite the decrease in the IC concentration of the SWW from 1500 ± 43 mg L^{-1} to 532 ± 24 mg L^{-1} during stage E, the IC concentration in the photobioreactor remained constant at 2236 ± 61 mg L^{-1}, which confirmed that a high alkalinity can be maintained in the cultivation broth using centrate as consequence of the high evaporation losses in the photobioreactor under favorable environmental conditions (Fig. 3b).

TN concentration recorded in the photobioreactor steadily increased from 65 mg N L^{-1} at the beginning of the experiment up to 556 mg L^{-1} by day 250 (Fig. S3a). This increase suggests that the nitrogen loading rate exceeded the nitrogen fixation rate by microalgae and was also promoted by the gradual increase of the evaporation rates. Nitrifying bacteria were responsible of the oxidation of NH_4^+ from the SWW used as a source of nutrients, to $N\text{-}NO_2^-$ and $N\text{-}NO_3^-$. In this sense, $N\text{-}NO_2^-$ concentration progressively

increased from stage A till the middle of stage C (day 144) up to 220 mg L^{-1} as consequence of the partial oxidation of NH_4^+ (Fig. S3b). However, a rapid decrease in the $N\text{-}NO_2^-$ concentration was observed from day 144 concomitantly with an increase in $N\text{-}NO_3^-$ concentration up to values of 440 mg L^{-1} by the end of stage E (Fig. S3c). The reasons underlying the partial nitrification of NH_4^+ at temperatures < 28 ºC in excess of DO during stages A and B, and the sudden increase in NO_2^- oxidation activity in stage C, remain unclear (Metcalf and Eddy, 2003).

On the contrary, $P\text{-}PO_4^{3-}$ concentrations recorded in the photobioreactor remained constant during stages A and B (109 mg L^{-1}), and gradually increased in stage C up to 263 mg L^{-1} concomitantly with the increase in water evaporation from the photobioreactor. In stage D the $P\text{-}PO_4^{3-}$ concentration further increased up to 395 mg L^{-1} and remained constant in stage E at 400 ± 7 mg L^{-1} (Fig. S4). The increase in $P\text{-}PO_4^{3-}$ concentration in stages D and E was likely due to the operation without greenhouse, which along with the higher temperatures of the cultivation broth, boosted water evaporation and the concentration of all dissolved salts in the medium.

Finally, an increase in the $S\text{-}SO_4^{2-}$ concentration of the photobioreactor from 123 mg L^{-1} at the beginning of stage A to 1027 mg L^{-1} by the end of stage E was recorded as result of the aerobic microbial oxidation of the H_2S. $S\text{-}SO_4^{2-}$ accumulation was also triggered with the increase in evaporation losses during stages D and E (Fig. S5). These $S\text{-}SO_4^{2-}$ concentrations were below the typical inhibitory thresholds for microbial activity reported in literature (74 g L^{-1}) (Lee et al., 2006; Muñoz et al., 2015).

3.3 Biogas upgrading

300 Eukaryotic algae and prokaryotic cyanobacteria were responsible of the bioconvertion of
301 the CO_2 present in biogas into biomass using the electrons released during water
302 photolysis, which entailed a concomitant release O_2. In this sense, the CO_2 concentration
303 of biomethane in stage A ranged between 1.9% and 4.9%, with CO_2 removal efficiencies
304 (REs) changing from 83.5% to 93.6% (Fig. 4a). During stage B, CO_2 concentration varied
305 from 2.4% to 6.1%, with CO_2-REs between 79.7% and 92.0%. A decrease in CO_2
306 concentration from 2.6% to 0.3% was observed during stage C due to the pH increase
307 mediated by the injection of air, which entailed CO_2-REs between 91.4% and 98.7%.
308 Finally, CO_2 concentrations in stages D and E remained constant at 0.5%, which
309 corresponded to CO_2-REs of 98.2% (Fig. 4a). The high CO_2 removal efficiencies
310 observed in stages C to E were supported by the high pH and buffer capacity of the
311 cultivation broth under the prevailing operational conditions. These values here achieved
312 were higher than those reported by Rodero et al., (2020), who observed CO_2
313 concentrations between 1.5 and 4.4% in a similar indoors experimental set-up with a
314 higher IC concentration in the cultivation broth (1203-3814 mg L^{-1}). It should be also
315 stressed that the CO_2-REs observed in stages A to C were higher than those previously
316 described during winter by Marín et al., (2018a), who recorded CO_2 REs between 63.6%
317 and 85.9% in a similar outdoors photobioreactor configuration during winter without
318 greenhouse. Therefore, these results validated the use of greenhouses and the injection of
319 air during winter conditions in order to enhance the CO_2-REs. The CO_2 concentrations
320 achieved in stages C, D and E fulfilled with the current legislation on the use of biogas
321 ($CO_2 \leq$ 2-4%) (European Committee for Standardization, 2018, 2017; Muñoz et al.,
322 2015).
323

H_2S was completely removed from biogas regardless of the operational conditions tested. H_2S was transferred from biogas to the algal-bacterial cultivation broth in the scrubbing column, where it was oxidized into SO_4^{2-} by aerobic sulphur oxidizing bacteria using the dissolved oxygen contained in the recirculating broth. The main biological mechanism of H_2S oxidation into SO_4^{2-} can be described by the following equation:

$$H_2S + CO_2 + N,P + O_2 \rightarrow biomass + S/SO_4^{2-} + H_2O$$

In addition, direct chemical oxidization into sulphate could also occur. This complete elimination was associated to the higher H_2S aqueous solubility (Henry´s law constant = C_L/C_G) compared to that of CO_2. Indeed, H_{H2S} is approximately three times higher than the H_{CO2} (Sander, 2015). These results were in accordance to Marín et al., (2018a), who reported a complete removal of H_2S in a similar outdoors photobioreactor configuration without greenhouse.

The N_2 concentration in biomethane in stages A and B remained constant at average values of 2.6 ± 0.5%. Interestingly, air stripping induced a reduce in the N_2 concentration from 2.5% to 1.0% during stage C, which remained constant at an average value of 1.7 ± 0.3% in stages D and E (Fig. 4b). This decrease in N_2 concentration at a constant L/G ratio might be explained by a decrease in the N_2 dissolved in the photobioreactor as consequence of the gradual increase in the salinity of the cultivation broth (ultimately induced by the increasing water evaporations). The N_2 concentrations here obtained were lower than those reported by Marín et al., (2018a), who recorded N_2 concentration values of up to 5.8% in a similar outdoors photobioreactor configuration during winter time at a L/G of 1.

The O_2 concentration recorded in biomethane exhibited a similar behavior than that observed for N_2. Thus, O_2 concentration remained constant at an average value of 1.0 ± 0.3% during stages A and B, and decreased to 0.4% during stage C. Similarly, the O_2 concentration remained constant in stages D and E at average values of 0.4 ± 0.1% (Fig. 4b). The decrease in biomethane O_2 concentrations from stage C to E was likely induced by the lower DO present in the cultivation broth used as scrubbing solution in the biogas absorption column. The biomethane O_2 concentration here reported fulfilled with the current legislation on the use of biogas which demands O_2 levels $\leq$ 1% (European Committee for Standardization, 2018, 2017; Muñoz et al., 2015).

Finally, CH_4 concentration recorded in biomethane ranged from 91.5% to 94.4% in stage A, 89.5% to 94.6% in stage B, 93.0% to 98.2% in stage C, 96.3% to 97.6% in stage D and 97.0% to 97.9% in stage E (Fig. 4c). The high CH_4 concentration obtained during winter conditions compared to previous studies was due to the high capacity of the system to remove CO_2 while preventing an active desorption of N_2 and O_2. Negligible losses of CH_4, lower than 1% of the CH_4 input, were recorded as a result of the low aqueous solubity of methane ($H_{CH4} \approx 0.03$ at 25 ºC). In addition, the presence of aerobic conditions likely supported the growth of methanotrophs, which prevented CH_4 emission from the cultivation broth in the photobioreactor (Muñoz et al., 2015; Serejo et al., 2015). The biogas upgrading performance here achieved was superior to that reported by Marín et al., (2020), who observed CH_4 concentrations up to 94.6% in a similar outdoors experimental set-up without greenhouse during autumn at a L/G of 1. The CH_4 concentrations obtained in the upgraded biogas also fulfilled with the current legislation

373 on the use of biogas (European Committee for Standardization, 2018, 2017; Muñoz et al.,
374 2015).

375 **<Figure 4>**

376

377 **3.4 Microalgae biomass parameters**

378 The VSS concentration in the photobioreactor increased from 0.14 g L^{-1} at day one to
379 0.53 g L^{-1} at the end of stage A. This increase was due to the fact that no biomass
380 harvesting was conducted in order to reach a pre-determined biomass concentration in
381 this stage (Fig. 5a; Table 1). In stage B, this concentration decreased to steady state values
382 of 0.30 g L^{-1} as a result of the constant withdrawal of biomass to maintain a biomass
383 productivity of 7.5 g m^{-2} d^{-1}. By the end of stage C, an increase in biomass concentration
384 up 0.83 g L^{-1} was observed, which was supported by the more favorable environmental
385 conditions. Similarly, an increased in biomass concentration up to 1.34 g L^{-1} was observed
386 by the end of stage D regardless of the increase in biomass withdrawal to 15 g m^{-2} d^{-1}.
387 Finally, an average VSS concentration of 1.25 g L^{-1} was recorded in stage E (Fig. 5a). At
388 this point, it is important to highlight that the VSS concentration during each stage was
389 determined by the predominanting environmental conditions and biomass productivity
390 imposed in each stage (Table 1). The greenhouse provided the local environmental
391 conditions in the photobioreactor to maintain higher VSS concentrations in the
392 photobioreactor during the winter months than those reported by Marín et al., (2018a) in
393 a similar photobioreactor.

394 **<Figure 5>**

395 The structure of the microalgal inoculum was gradually replaced by a microalgae
396 assemblage composed of *Mychonastes homosphaera* (78%) and *Navicula sp.* (22%)
397 during stage A (October) (Fig. 5b). In stage B, *Mychonastes homosphaera* was the

dominant microalga in the consortium, accounting for a share of 95% in November, 61% in December and 100% in January. The dominant microalgae by the end of stage C was *Pseudanabaena sp.* (66%) and *Mychonastes homosphaera* (34%) (April). Interestingly, *Mychonastes homosphaera* represented 99% of the microalgae population and *Pseudanabaena sp.* accounted only for 1% (May) in stage D. Finally, the microalgae assemblage in stage E was composed of *Mychonastes homosphaera* (92%) and *Scenedesmus sp.* (8%) (June) (Fig. 5b). It's important to highlight the fact that ambient temperature and PAR were the most important environmental parameters determining the microalgae population structure prevailing in the photobioreactor, which were directly impacted by the use of a greenhouse during stages A to C. Temperature induce an exponential influence on the bioreactions occurring in microalgae, which ultimately determine the specific microalgae growth rate and the dominance of a microalga species under continuous cultivation. Variations in temperature can also affect the magnitude of algal nutrients uptake and therefore the phytoplankton growth processes can be indirectly affected (Beardall and Stojkovic, 2006). The PAR controls microalgae growth rate, inducing the inhibition of photosynthesis at high light intensities in some species, which would result in changes in the dominant species in the system (Beardall and Stojkovic, 2006). The use of tap water or Na_2CO_3/$NaHCO_3$ supplemented SWW in order to compensate water evaporation also modified the characteristics of the cultivation broth (in terms of salinity), which likely impacted microalgae growth. Finally, process operation under different biomass productivities (set by controlling the biomass wastage rate from the settler) likely influenced the microalgae population structure. However, the changes in microalgae population structure along the experiment were not correlated to biogas upgrading efficiency, since photosynthetic activity was actively maintained regardless of the dominant microalgae species. Indeed, different CO_2 removal

423 efficiencies and CH_4 contents were recorded in November and June or January and May
424 under similar microalgae population structures.
425
426 An analysis of the N and P fixed and oxidized by the algal-bacterial biomass was
427 conducted and summarized in Table 2. A share of 34 ± 5, 83 ± 5, 88 ± 3, 50 ± 8 and 39
428 ± 5% of the nitrogen supplied with the SWW was fixed into biomass at stages A to E,
429 respectively. Similarly, the share of the input nitrogen oxidized into NO_2^- and NO_3^-
430 accounted for 66 ± 6, 12 ± 3, 29 ± 4, 16 ± 3 and 3 ± 1% in stages A, B, C, D and E,
431 respectively. Similarly, a share of 32 ± 3, 62 ± 6, 53 ± 13, 30 ± 4 and 25 ± 4% of the
432 phosphate input was assimilated into biomass.
433 **<Table 2>**
434
435 **4. Conclusions**
436 This study proved for the first time the effectiveness of three innovative operational
437 strategies in an outdoors pilot photobioreactor interconnected to a biogas absorption unit
438 to overcome the main technical limitations of photosynthetic biogas upgrading. The use
439 of a greenhouse and direct CO_2 stripping in the photobioreactor via air stripping during
440 winter conditions, and the use of digestate as a make-up water during summer conditions
441 can provide a biomethane that fulfilled with the current legislation on the use of biogas.
442
443 **Acknowledgements**
444 This work was supported by FUNDACION DOMINGO MARTINEZ, the Regional
445 Government of Castilla y León and the EU-FEDER programme (CLU 2017-09 and UIC
446 071). The financial support of the Regional Government of Castilla y León is also
447 acknowledged for the PhD grant of David Marín.

448

449 **REFERENCES**

450 Angelidaki, I., Treu, L., Tsapekos, P., Luo, G., Campanaro, S., Wenzel, H., Kougias,
451 P.G., 2018. Biogas upgrading and utilization: Current status and perspectives.
452 Biotechnol. Adv. 36, 452–466. https://doi.org/10.1016/j.biotechadv.2018.01.011
453 APHA, 2005. Standard Methods for the Examination of Water and Wastewater, 21st ed.
454 Public Health Association, Washington DC.
455 Bahr, M., Díaz, I., Dominguez, A., González Sánchez, A., Muñoz, R., 2014.
456 Microalgal-biotechnology as a platform for an integral biogas upgrading and
457 nutrient removal from anaerobic effluents. Environ. Sci. Technol. 48, 573–581.
458 https://doi.org/10.1021/es403596m
459 Beardall, J., Stojkovic, S., 2006. Microalgae under Global Environmental Change :
460 Implications for Growth and Productivity , Populations and Trophic Flow.
461 Scienceasia 1, 1–10. https://doi.org/10.2306/scienceasia1513-
462 1874.2006.32(s1).001
463 Bose, A., Lin, R., Rajendran, K., O'Shea, R., Xia, A., Murphy, J.D., 2019. How to
464 optimise photosynthetic biogas upgrading: a perspective on system design and
465 microalgae selection. Biotechnol. Adv. 107444.
466 https://doi.org/10.1016/j.biotechadv.2019.107444
467 European Biogas Association, 2018. EBA Statistical Report 2018 [WWW Document].
468 URL https://www.europeanbiogas.eu/eba-statistical-report-2018/ (accessed
469 12.2.19).
470 European Committee for Standardization, 2018. UNE EN 16723-2:2018 Natural gas
471 and biomethane for use in transport and biomethane for injection in the natural gas
472 network - Part 2: Automotive fuels specification [WWW Document]. URL

https://www.en-standard.eu/une-en-16723-2-2018-natural-gas-and-biomethane-for-use-in-transport-and-biomethane-for-injection-in-the-natural-gas-network-part-2-automotive-fuels-specification/ (accessed 12.10.19).

European Committee for Standardization, 2017. UNE EN 16723-1:2017 Natural gas and biomethane for use in transport and biomethane for injection in the natural gas network - Part 1: Specifications for biomethane for injection in the natural gas network [WWW Document]. URL https://www.en-standard.eu/une-en-16723-1-2017-natural-gas-and-biomethane-for-use-in-transport-and-biomethane-for-injection-in-the-natural-gas-network-part-1-specifications-for-biomethane-for-injection-in-the-natural-gas-network/ (accessed 12.10.19).

Farooq, M., Almustapha, M.N., Imran, M., Saeed, M.A., Andresen, J.M., 2018. In-situ regeneration of activated carbon with electric potential swing desorption (EPSD) for the H2S removal from biogas. Bioresour. Technol. 249, 125–131. https://doi.org/10.1016/j.biortech.2017.09.198

Franco-Morgado, M., Alcántara, C., Noyola, A., Muñoz, R., González-Sánchez, A., 2017. A study of photosynthetic biogas upgrading based on a high rate algal pond under alkaline conditions: Influence of the illumination regime. Sci. Total Environ. 592, 419–425. https://doi.org/10.1016/j.scitotenv.2017.03.077

Lee, E.Y., Lee, N.Y., Cho, K.S., Ryu, H.W., 2006. Removal of hydrogen sulfide by sulfate-resistant Acidithiobacillus thiooxidans AZ11. J. Biosci. Bioeng. 101, 309–314. https://doi.org/10.1263/jbb.101.309

Marín, D., Carmona-Martínez, A.A., Lebrero, R., Muñoz, R., 2020. Influence of the diffuser type and liquid-to-biogas ratio on biogas upgrading performance in an outdoor pilot scale high rate algal pond. Fuel 275, 117999. https://doi.org/10.1016/j.fuel.2020.117999

Marín, D., Ortíz, A., Díez-Montero, R., Uggetti, E., García, J., Lebrero, R., Muñoz, R., 2019. Influence of liquid-to-biogas ratio and alkalinity on the biogas upgrading performance in a demo scale algal-bacterial photobioreactor. Bioresour. Technol. 280, 112–117. https://doi.org/10.1016/j.biortech.2019.02.029

Marín, D., Posadas, E., Cano, P., Pérez, V., Blanco, S., Lebrero, R., 2018a. Seasonal variation of biogas upgrading coupled with digestate treatment in an outdoors pilot scale algal-bacterial photobioreactor. Bioresour. Technol. 263, 58–66. https://doi.org/10.1016/j.biortech.2018.04.117

Marín, D., Posadas, E., Cano, P., Pérez, V., Lebrero, R., Muñoz, R., 2018b. Influence of the seasonal variation of environmental conditions on biogas upgrading in an outdoors pilot scale high rate algal pond. Bioresour. Technol. 255, 354–358. https://doi.org/10.1016/j.biortech.2018.01.136

Metcalf, Eddy, 2003. Wastewater Engineeering and Reuse. Mc GrawHill.

Molina, E., Ferna, J., Acie, F.G., Chisti, Y., 2001. Tubular photobioreactor design for algal cultures. J. Biotechnol. 92, 113–131.

Muñoz, R., Meier, L., Diaz, I., Jeison, D., 2015. A review on the state-of-the-art of physical/chemical and biological technologies for biogas upgrading. Rev. Environ. Sci. Bio/Technology 14, 727–759. https://doi.org/10.1007/s11157-015-9379-1

Nagarajan, D., Lee, D.-J., Chang, J.-S., 2019. Integration of anaerobic digestion and microalgal cultivation for digestate bioremediation and biogas upgrading. Bioresour. Technol. 290, 121804. https://doi.org/10.1016/j.biortech.2019.121804

Posadas, E., García-Encina, P.A., Soltau, A., Domínguez, A., Díaz, I., Muñoz, R., 2013. Carbon and nutrient removal from centrates and domestic wastewater using algal-bacterial biofilm bioreactors. Bioresour. Technol. 139, 50–58. https://doi.org/10.1016/j.biortech.2013.04.008

Posadas, E., Marín, D., Blanco, S., Lebrero, R., Muñoz, R., 2017. Simultaneous biogas upgrading and centrate treatment in an outdoors pilot scale high rate algal pond. Bioresour. Technol. 232, 133–141. https://doi.org/10.1016/j.biortech.2017.01.071

Posadas, E., Serejo, M.L., Blanco, S., Pérez, R., García-Encina, P.A., Muñoz, R., 2015. Minimization of biomethane oxygen concentration during biogas upgrading in algal-bacterial photobioreactors. Algal Res. 12, 221–229. https://doi.org/10.1016/j.algal.2015.09.002

Posadas, E., Szpak, D., Lombó, F., Domínguez, A., Díaz, I., Blanco, S., García-Encina, P.A., Muñoz, R., 2016. Feasibility study of biogas upgrading coupled with nutrient removal from anaerobic effluents using microalgae-based processes. J. Appl. Phycol. 28, 2147–2157. https://doi.org/10.1007/s10811-015-0758-3

Rodero, M. del R., Severi, C.A., Rocher-Rivas, R., Quijano, G., Muñoz, R., 2020. Long-term influence of high alkalinity on the performance of photosynthetic biogas upgrading. Fuel 281, 118804. https://doi.org/10.1016/j.fuel.2020.118804

Rodero, R., Ángeles, R., Marín, D., Díaz, I., Colzi, A., Posadas, E., Lebrero, R., Muñoz, R., 2018a. Biogas Purification and Upgrading Technologies, in: Tabatabaei, M., Ghanavati, H. (Eds.), Biogas: Fundamentals, Process, and Operation. Springer International Publishing, pp. 239–276. https://doi.org/10.1007/978-3-319-77335-3

Rodero, R., Lebrero, R., Serrano, E., Lara, E., Arbib, Z., García-Encina, P.A., Muñoz, R., 2019. Technology validation of photosynthetic biogas upgrading in a semi-industrial scale algal-bacterial photobioreactor. Bioresour. Technol. 279, 43–49. https://doi.org/10.1016/j.biortech.2019.01.110

Rodero, R., Posadas, E., Toledo-Cervantes, A., Lebrero, R., Muñoz, R., 2018b. Influence of alkalinity and temperature on photosynthetic biogas upgrading efficiency in high rate algal ponds. Algal Res. 33, 284–290.

548 https://doi.org/10.1016/j.algal.2018.06.001
549 Ryckebosch, E., Drouillon, M., Vervaeren, H., 2011. Techniques for transformation of
550 biogas to biomethane. Biomass and Bioenergy 35, 1633–1645.
551 https://doi.org/10.1016/j.biombioe.2011.02.033
552 Sander, R., 2015. Compilation of Henry ’s law constants (version 4.0) for water as
553 solvent 4399–4981. https://doi.org/10.5194/acp-15-4399-2015
554 Serejo, M.L., Posadas, E., Boncz, M.A., Blanco, S., García-Encina, P., Muñoz, R.,
555 2015. Influence of biogas flow rate on biomass composition during the
556 optimization of biogas upgrading in microalgal-bacterial processes. Environ. Sci.
557 Technol. 49, 3228–3236. https://doi.org/10.1021/es5056116
558 Sournia, A., 1978. Phytoplankton manual.
559 Stürmer, B., Kirchmeyr, F., Kovacs, K., Gba, F.H., Rea, D.C., Atee, I., Eba, J.S.,
560 Proietti, S., 2016. Technical-economic analysis for determining the feasibility
561 threshold for tradable biomethane certificates [WWW Document]. URL
562 http://www.ergar.org/wp-content/uploads/2018/07/BIOSURF-D3.4.pdf (accessed
563 6.1.20).
564 Toledo-cervantes, A., Estrada, J.M., Lebrero, R., Muñoz, R., 2017. A comparative
565 analysis of biogas upgrading technologies : Photosynthetic vs physical / chemical
566 processes. Algal Res. 25, 237–243. https://doi.org/10.1016/j.algal.2017.05.006
567 Toledo-Cervantes, A., Serejo, M.L., Blanco, S., Pérez, R., Lebrero, R., Muñoz, R.,
568 2016. Photosynthetic biogas upgrading to bio-methane: Boosting nutrient recovery
569 via biomass productivity control. Algal Res. 17, 46–52.
570 https://doi.org/10.1016/j.algal.2016.04.017
571 Utermöhl, H., 1958. Zur vervollkommnung der quantitativen phytoplankton-methodik:
572 mit 1 Tabelle und 15 abbildungen im Text und auf 1 Tafel, in: Internationale

573 Vereinigung Für Theoretische Und Angewandte Limnologie: Mitteilungen. pp. 1–
574 38.
575

FIGURE CAPTIONS

Figure 1. Schematic diagram of the outdoors experimental pilot plant used for the continuous photosynthetic upgrading of biogas.

Figure 2. Time course of (a) ambient temperature, (b) temperature inside the greenhouse (c) photobioreactor temperature, (d) ambient PAR and (e) PAR inside the greenhouse during the morning (solid symbols) and afternoon (empty symbols).

Figure 3. Time course of the (a) pH in the photobioreactor and (b) concentration of inorganic carbon in the SWW (■) and in the photobioreactor (○).

Figure 4. Time course of the concentration of (a) CO_2 (■), (b) N_2 (△) and O_2 (◆), and (c) CH_4 (○) in the upgraded biogas.

Figure 5. Time course of the (a) concentration of volatile suspended solids in the photobioreactor and (b) structure of microalgae population in the photobioreactor.

Figure 1. Schematic diagram of the outdoors experimental pilot plant used for the continuous photosynthetic upgrading of biogas.

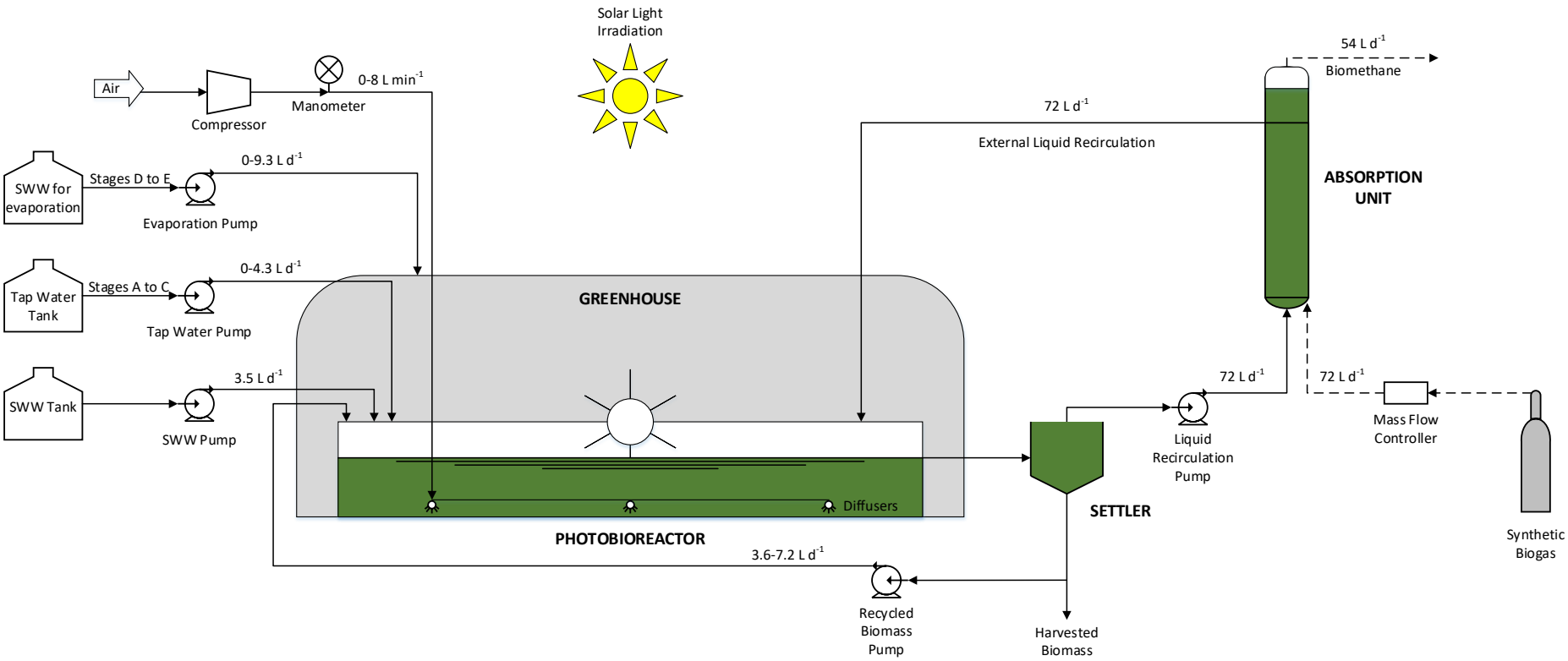

Figure 2. Time course of (a) ambient temperature, (b) temperature inside the greenhouse (c) photobioreactor temperature, (d) ambient PAR and (e) PAR inside the greenhouse during the morning (solid symbols) and afternoon (empty symbols).

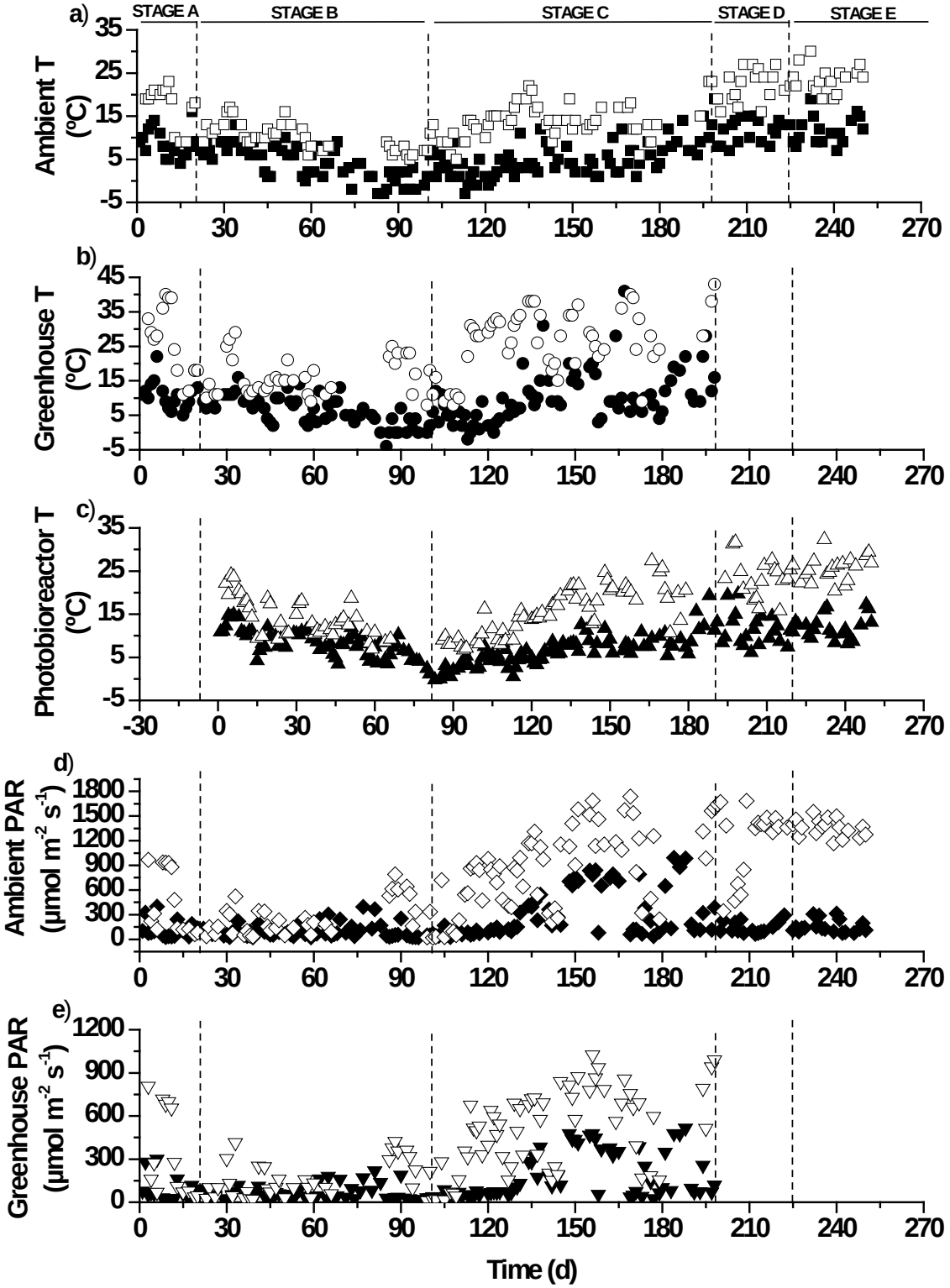

Figure 3. Time course of the (a) pH in the photobioreactor and (b) concentration of inorganic carbon in the SWW (■) and in the photobioreactor (○).

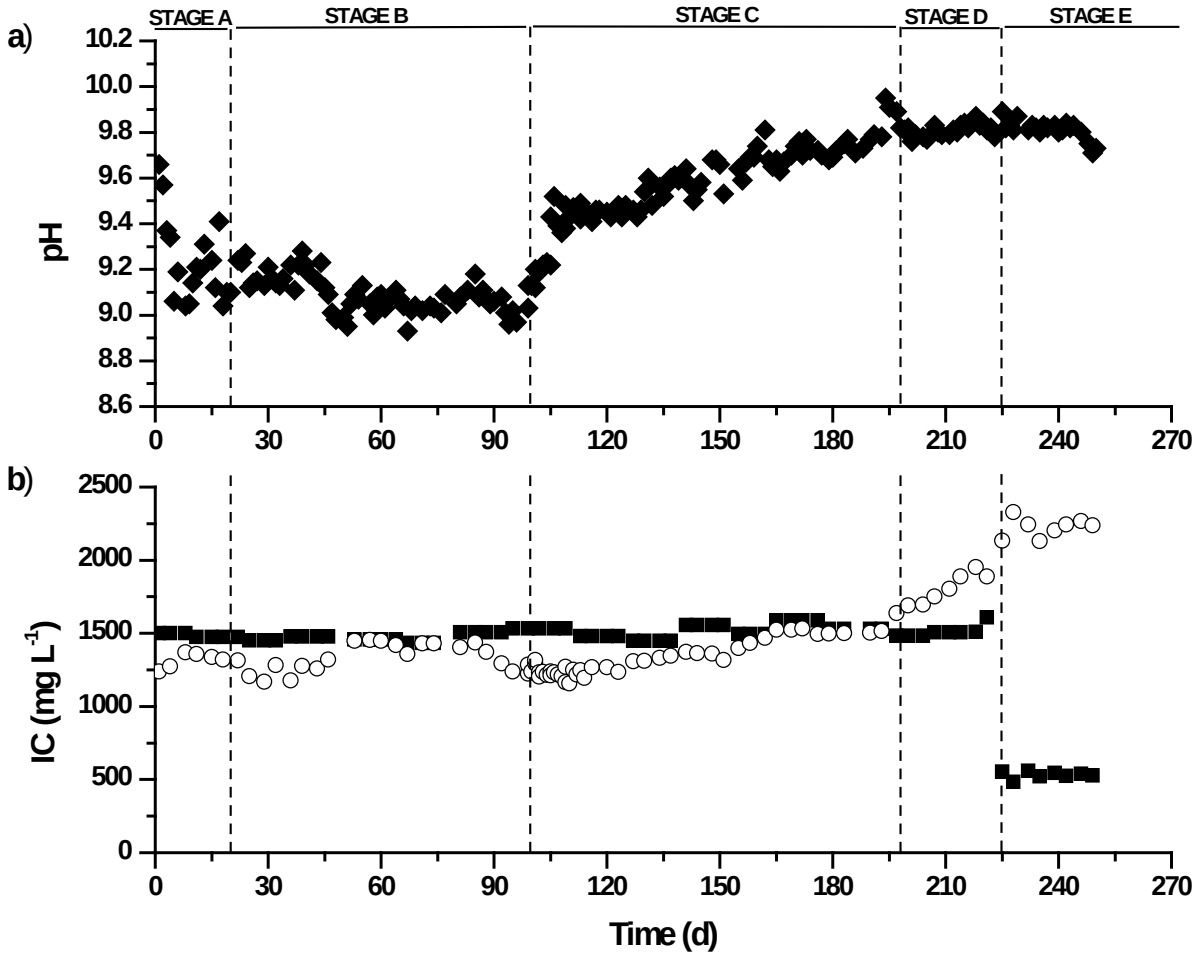

Figure 4. Time course of the concentration of (a) CO_2 (■), (b) N_2 (△) and O_2 (◆), and (c) CH_4 (○) in the upgraded biogas.

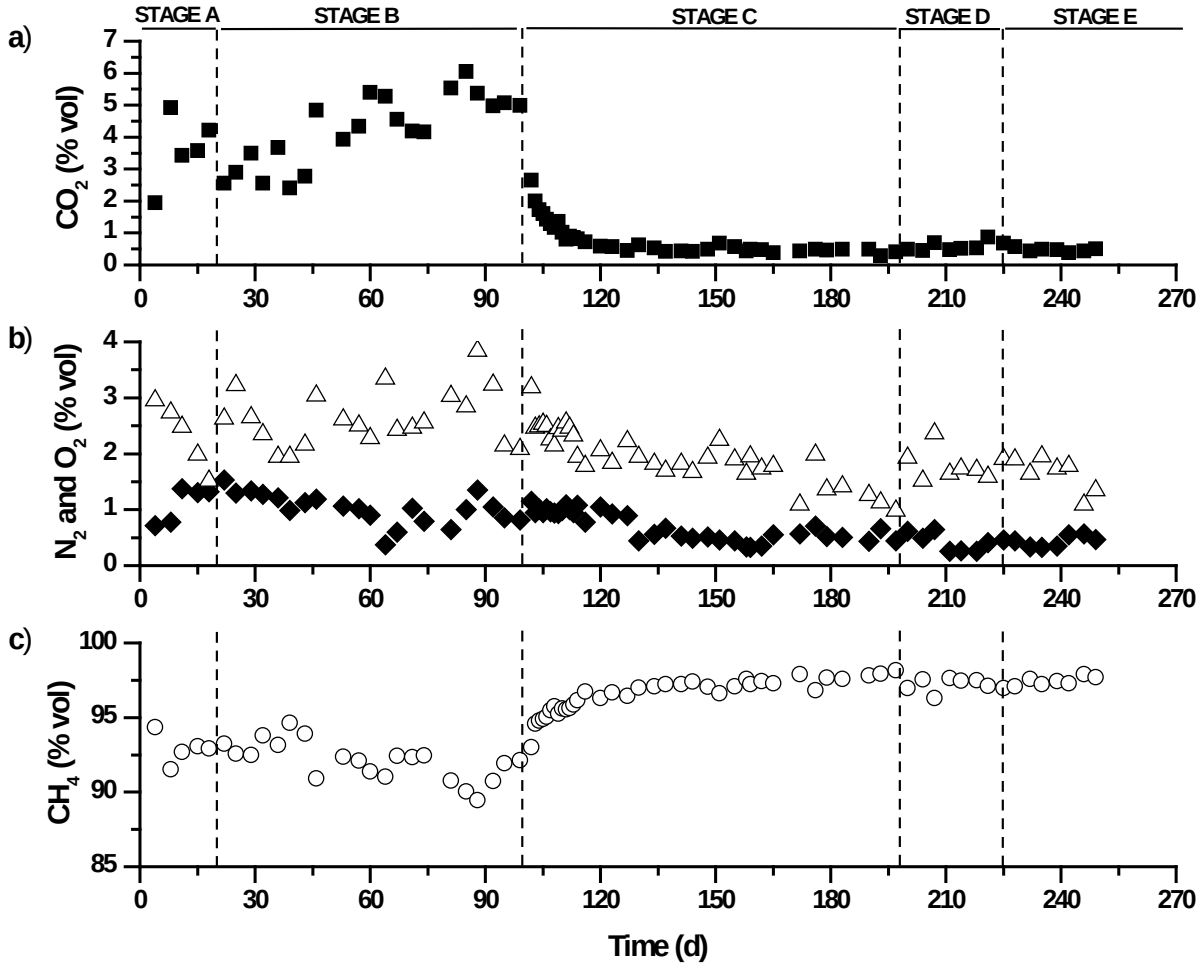

Figure 5. Time course of the (a) concentration of volatile suspended solids in the photobioreactor and (b) structure of microalgae population in the photobioreactor.

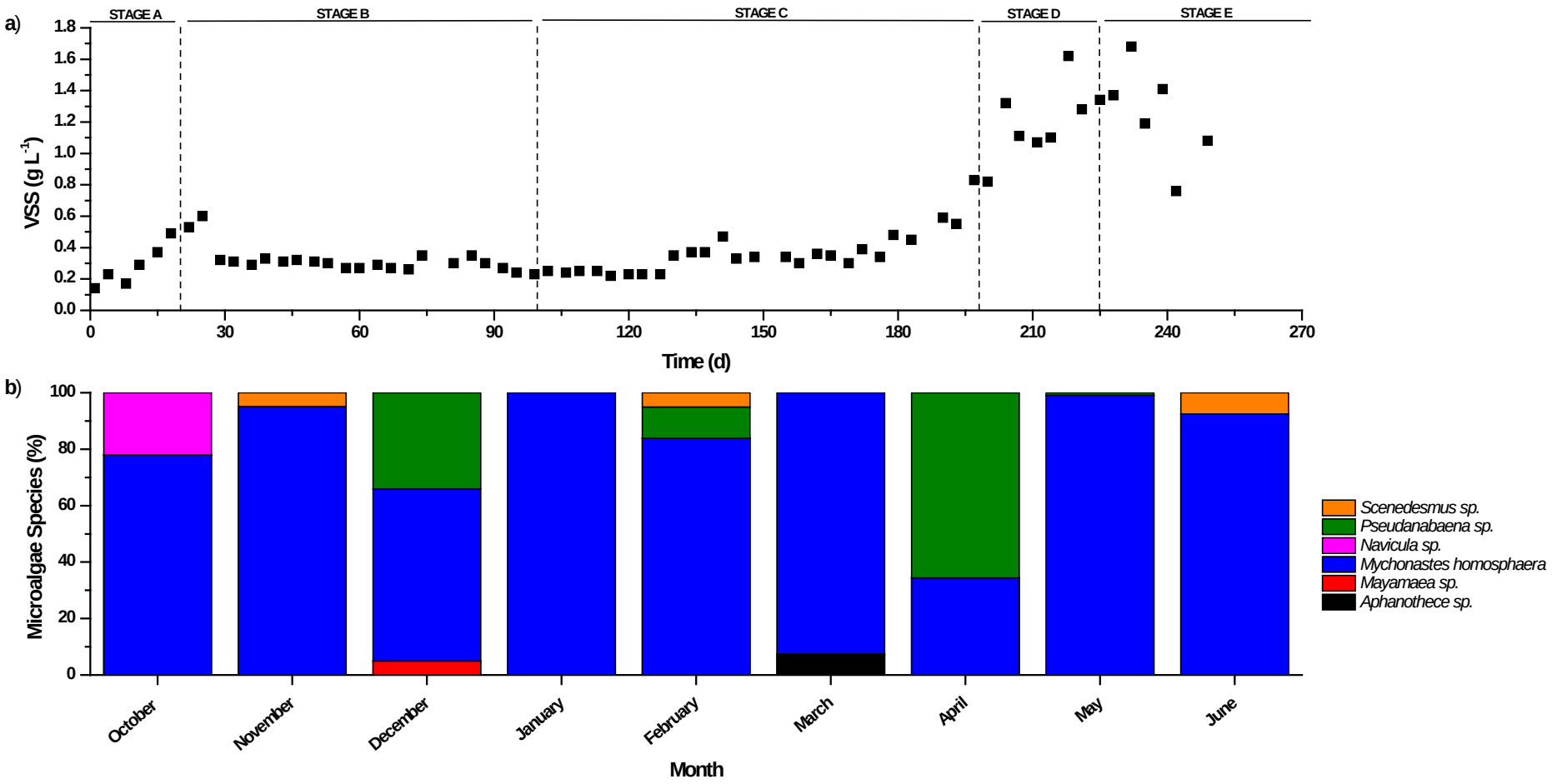

Table 1. Environmental and operational parameters during the five operational stages.

	Stage				
Parameter	**A**	**B**	**C**	**D**	**E**
Date	15-Oct – 04-Nov	05-Nov – 20-Jan	21-Jan – 30-Apr	01-May – 27-May	28-May – 21-Jun
Stage period (approx. weeks)	3	11	14	3	4
Use of Greenhouse	Yes	Yes	Yes	No	No
Air Supply ($L\ min^{-1}$)	0.0	0.0	8.0	8.0	0.0
Make up water ($L\ d^{-1}$)	0.5 ± 0.2 (Tap water)	0.0 ± 0.0 (Tap water)	1.1 ± 1.2 (Tap water)	2.8 ± 1.4 (SWW)	5.2 ± 1.4 (SWW*)
Morning Average DO ($mg\ L^{-1}$)	8.2 ± 2.2	9.2 ± 1.7	10.6 ± 0.8	9.8 ± 0.7	7.7 ± 0.6
Afternoon Average DO ($mg\ L^{-1}$)	12.5 ± 5.5	12.8 ± 1.4	9.2 ± 1.1	8.2 ± 0.2	7.3 ± 0.3
Average Evaporation Rate ($L\ m^{-2}\ d^{-1}$)	1.7 ± 1.2	1.1 ± 0.4	2.4 ± 1.0	5.2 ± 1.2	7.3 ± 1.1
Biomass productivity ($g\ m^{-2}\ d^{-1}$)	0.0	7.5	7.5	15.0	15.0

*- SWW with an inorganic carbon concentration of 532 ± 24 mg C L^{-1}

Table 2. Nutrient recovery via biomass assimilation.

Stage	N		P
	Fixed (%)	**Oxidized (%)**	**Fixed (%)**
A	34 ± 5	66 ± 6	32 ± 3
B	83 ± 5	12 ± 3	62 ± 6
C	88 ± 3	29 ± 4	53 ± 13
D	50 ± 8	16 ± 3	30 ± 4
E	39 ± 5	3 ± 1	25 ± 4

APPENDIX

Innovative operational strategies in photosynthetic biogas upgrading in an outdoors pilot scale algal-bacterial photobioreactor

David Marín[1, 2, 3], Alessandro A. Carmona-Martínez[1, 2], Saúl Blanco[4], Raquel Lebrero[1, 2], Raúl Muñoz*[1, 2]

[1] Department of Chemical Engineering and Environmental Technology, School of Industrial Engineering, Valladolid University, Dr. Mergelina, s/n, 47011, Valladolid, Spain.

[2] Institute of Sustainable Processes, Dr. Mergelina, s/n, 47011, Valladolid, Spain.

[3] Universidad Pedagógica Nacional Francisco Morazán, Boulevard Centroamérica, Tegucigalpa, Honduras.

[4] Department of Biodiversity and Environmental Management, University of León, 24071 León, Spain.

* Corresponding author: mutora@iq.uva.es

Environmental parameters

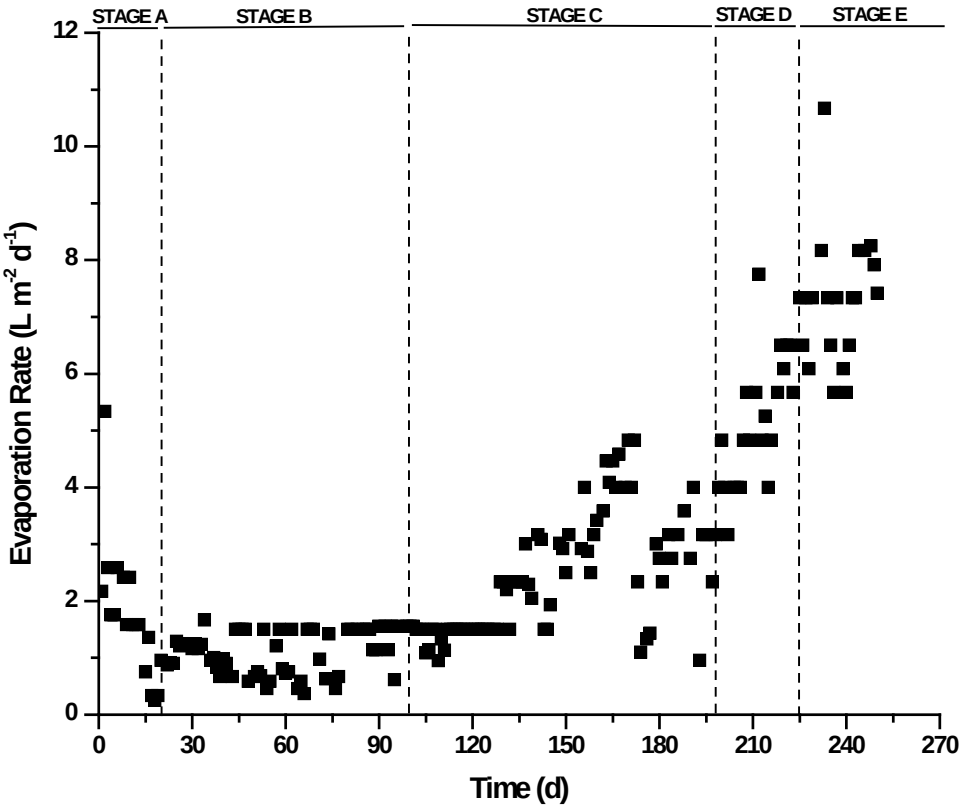

Figure S1. Time course of the evaporation rate in the photobioreactor.

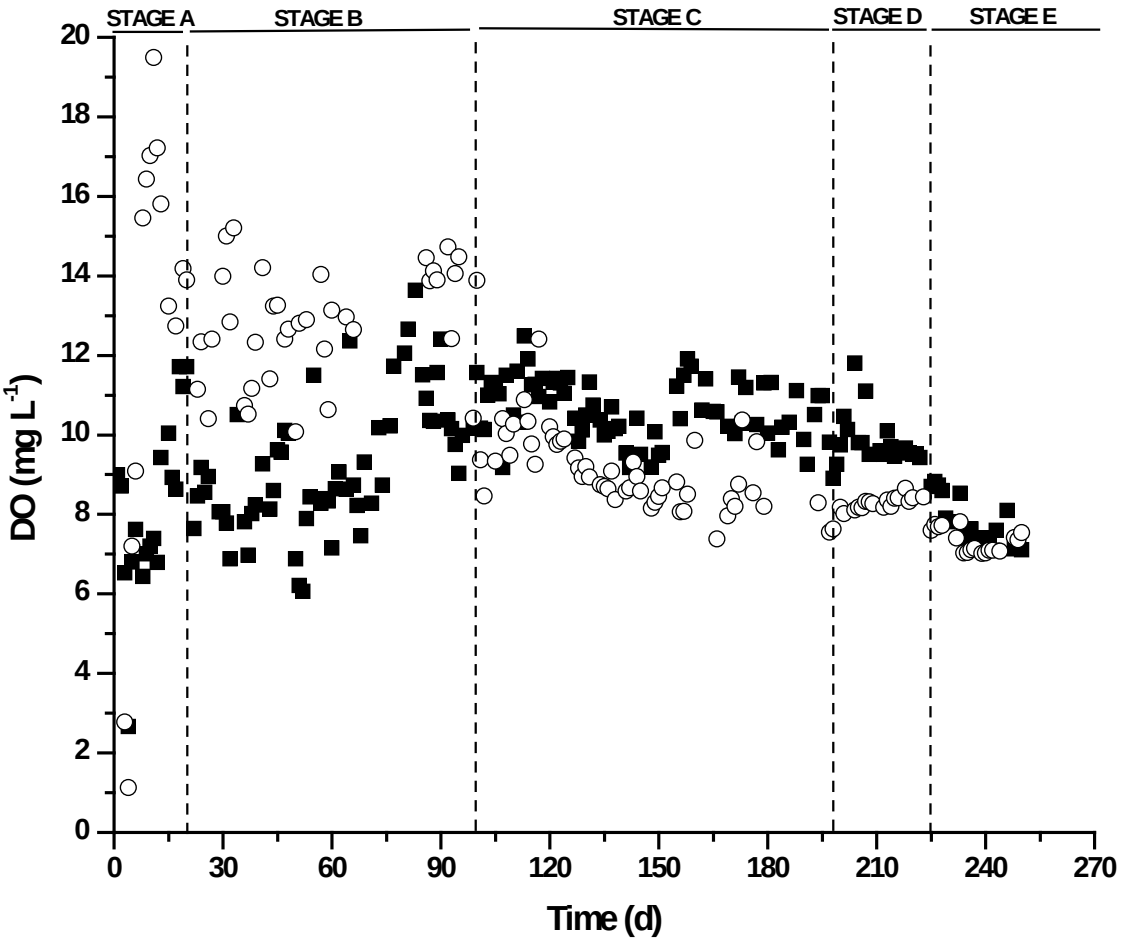

Figure S2. Time course of the dissolved oxygen concentration in the photobioreactor in the morning (solid symbols) and afternoon (empty symbols).

25 **Cultivation broth parameters**

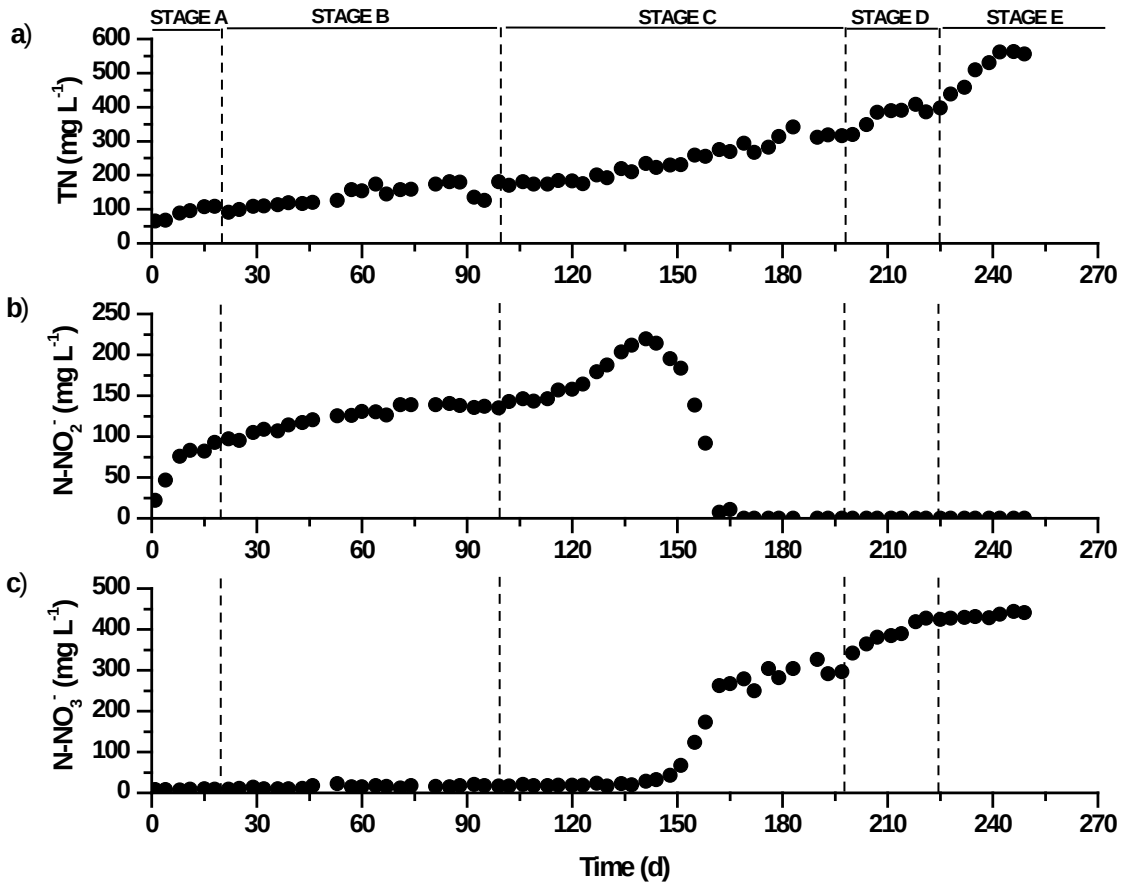

26

27 **Figure S3.** Time course of the concentration of (a) total nitrogen, (b) $N\text{-}NO_2^-$ and (c) $N\text{-}NO_3^-$ in the photobioreactor.

28

29

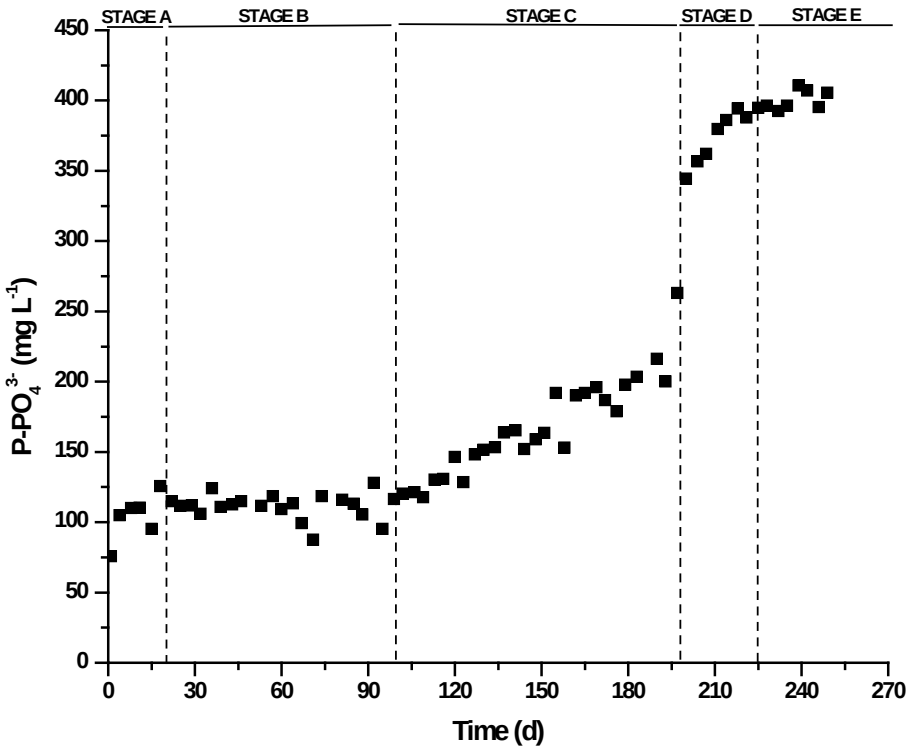

Figure S4. Time course of the concentration of $P\text{-}PO_4^{3-}$ in the photobioreactor.

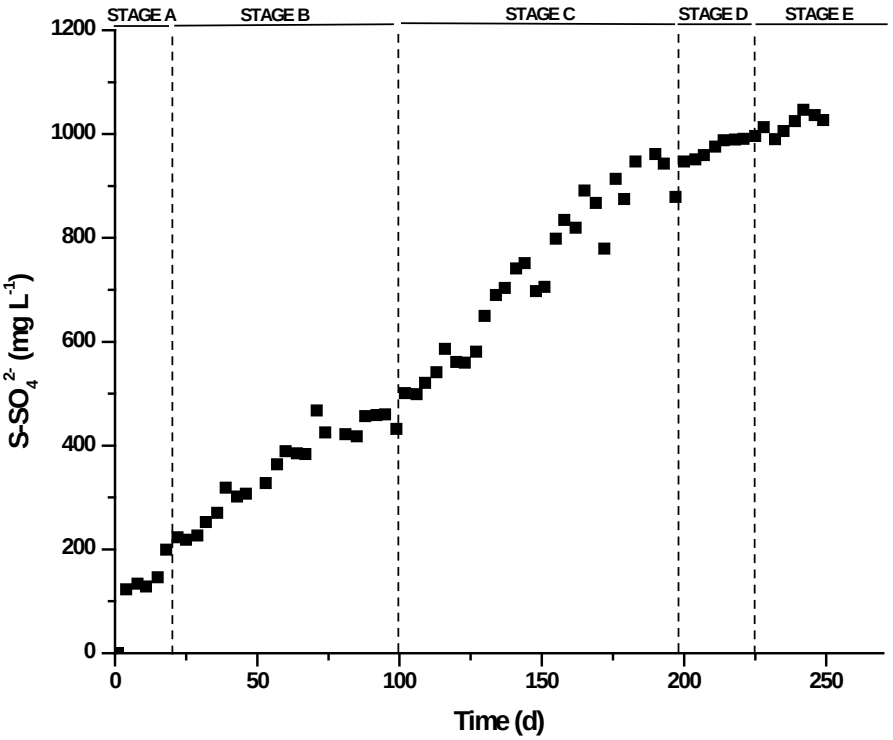

Figure S5. Time course of the concentration of $S\text{-}SO_4^{2-}$ in the photobioreactor.